

ProSTformer: Pre-trained Progressive Space-Time Self-attention Model for Traffic Flow Forecasting

Xiao Yan,¹ Xianghua Gan,¹ Jingjing Tang¹ Rui Wang¹

¹ School of Business Administration, Faculty of Business Administration, Southwestern University of Finance and Economics.

Abstract

Traffic flow forecasting is essential and challenging to intelligent city management and public safety. Recent studies have shown the potential of convolution-free Transformer approach to extract the dynamic dependencies among complex influencing factors. However, two issues prevent the approach from being effectively applied in traffic flow forecasting. First, it ignores the spatiotemporal structure of the traffic flow videos. Second, for a long sequence, it is hard to focus on crucial attention due to the quadratic times dot-product computation. To address the two issues, we first factorize the dependencies and then design a progressive space-time self-attention mechanism named ProSTformer. It has two distinctive characteristics: (1) corresponding to the factorization, the self-attention mechanism progressively focuses on spatial dependence from local to global regions, on temporal dependence from inside to outside fragment (i.e., closeness, period, and trend), and finally on external dependence such as weather, temperature, and day-of-week; (2) by incorporating the spatiotemporal structure into the self-attention mechanism, each block in ProSTformer highlights the unique dependence by aggregating the regions with spatiotemporal positions to significantly decrease the computation. We evaluate ProSTformer on two traffic datasets, and each dataset includes three separate datasets with big, medium, and small scales. Despite the radically different design compared to the convolutional architectures for traffic flow forecasting, ProSTformer performs better or the same on the big scale datasets than six state-of-the-art baseline methods by RMSE. When pre-trained on the big scale datasets and transferred to the medium and small scale datasets, ProSTformer achieves a significant enhancement and behaves best.

1 Introduction

Traffic flow forecasting plays a vital role in traffic control, vehicle scheduling, and risk assessment (Zheng et al. 2014). For example, it is indispensable for congestion alleviation and real-time control of traffic signals in intelligent cities. In bike-sharing systems, bike flow forecasting is crucial for operators to rebalance bikes from oversupplied regions to undersupplied regions. It is a standard forecasting approach to generate flow videos for partitioned city regions and then leverage flow videos and external factors

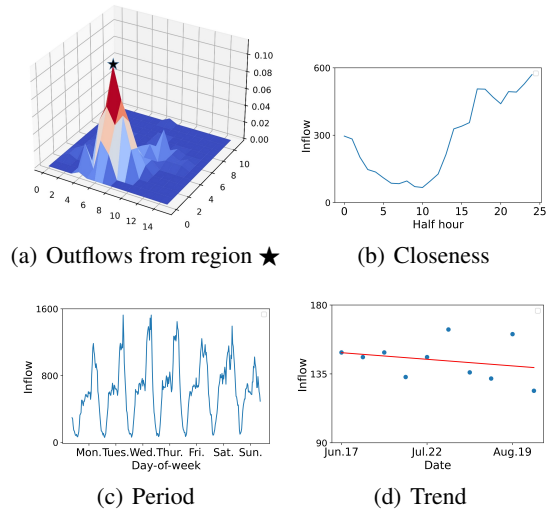


Figure 1: The spatial dependence and temporal dependence. (a) reflects the local and global spatial dependencies. (b), (c), and (d) reflect the temporal dependencies of closeness, period, and trend, specifically, (b) shows that flows are relevant to recent time intervals; (c) shows that flows during certain hours are similar on consecutive days; (d) shows that long-term flows progressively decrease from June to August.

such as weather conditions, wind speed, temperature, and day-of-week. Works using this approach include Zhang et al. (2016), Zhang, Zheng, and Qi (2017), Ke et al. (2017), Yao et al. (2018), Zhang, Liu, and Zheng (2019), Du et al. (2019), and Chen et al. (2021). These studies adopt various convolutional networks to extract the dynamic spatiotemporal dependence. Recently, Duan et al. (2019) and Lin et al. (2019) not only use various convolutional networks, but also introduce Transformer to construct model architecture for traffic flow forecasting. In these studies, Transformer is applied in conjunction with convolutional networks. Dosovitskiy et al. (2020) show that the reliance on convolutional networks is not necessary and a pure Transformer network applied directly to sequences of image patches can effectively extract the spatiotemporal dependence. When pre-trained on large amounts of data and transferred to multiple mid-sized or

small image recognition benchmarks, Transformer performs similar to or better than state-of-the-art convolutional networks. This study shows the potential of convolution-free Transformer approach for traffic flow forecasting.

However, two significant issues prevent the pure Transformer from being effectively applied in traffic flow forecasting. First, Transformer does not incorporate spatiotemporal structure of flow videos into self-attention mechanism. Take NYCTaxi dataset as an example, Figure 1(a) depicts outflows from region \star to itself and other regions from 6 PM to 7 PM. The percentages of the outflows from \star to itself, from \star to adjacent regions (i.e., the surrounding 14 regions), and from \star to distant regions (i.e., other 28 nonzero regions) are about 11%, 64%, and 25%, respectively. Figure 1(b), 1(c), and 1(d) show temporal dependencies of closeness, period, and trend, respectively. The spatiotemporal structure, which reflects the local and global spatial dependencies and temporal correlations among different time intervals, is ignored in Transformer architecture. Second, by splitting the flow videos into a long sequence of patches, a large part of low relevant patches make the traditional self-attention mechanism hard to focus on crucial attention due to the quadratic times dot-product computation.

To address the two issues, we factorize the dependencies into local-global spatial dependence, inside-outside temporal dependence, and external dependence such as weather, temperature, and day-of-week. Corresponding to the factorization, we propose a progressive space-time self-attention mechanism named ProSTformer. It progressively focuses on spatial dependence from local to global regions, on temporal dependence from inside to outside fragment (i.e., closeness, period, and trend), and finally on external dependence. In ProSTformer, each block highlights the unique dependence by aggregating the regions with spatiotemporal positions to significantly decrease the computation.

There are some prior works on improving the efficiency of self-attention to alleviate issue 2. Sparse Transformer (Child et al. 2019), LogSparse Transformer (Li et al. 2019), Longformer (Beltagy, Peters, and Cohan 2020), Reformer (Kitaev, Kaiser, and Levskaya 2020), and Informer (Zhou et al. 2021) focus on reducing the complexity of the self-attention mechanism. E.g., Informer designs a ProbSparse self-attention mechanism distilling highlights dominating self-attention by halving cascading layer input and efficiently handles extreme long input sequences. TimeSformer (Bertasius, Wang, and Torresani 2021) use a divided time-space self-attention mechanism on video classification tasks to decrease the computation.

The contributions of this paper are summarized as follows:

- We propose a progressive space-time self-attention mechanism named ProSTformer that can enhance the prediction capacity in traffic flow forecasting problem. We also show the convolution-free Transformer-like model’s potential value to capture spatiotemporal dependence in traffic flow forecasting.
- ProSTformer incorporates the structure information of input. In ProSTformer, each block highlights the unique

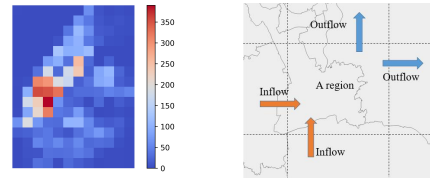
dependence by aggregating the regions with spatiotemporal positions to significantly decreases the computation.

- We conduct data augmentation tasks for ProSTformer, and show that closely relevant and large amounts of data pre-training both are of great importance for traffic flow forecasting.

2 Preliminary

We first define the problem of traffic flow forecasting.

Definition 1. (Region and time partition (Zhang et al. 2016)) The city area is partitioned into $I \times J$ grids uniformly based on the longitude and latitude where a grid denotes a region, as shown in Figure 2.



(a) Outflow matrix by half-hour (b) Inflow and outflow

Figure 2: Regions in New York City

Definition 2. (Inflow/outflow (Zhang et al. 2016)) Let R be a collection of trajectories at the t^{th} time interval. For a grid (i, j) that lies at the i^{th} row and the j^{th} column, the inflows and outflows at time interval t are defined respectively as:

$$x_t^{\text{in},i,j} = \sum_{Tr \in R} |\{k \geq 1 \mid g_k^{\text{end}} \in (i, j)\}|$$

$$x_t^{\text{out},i,j} = \sum_{Tr \in R} |\{k \geq 1 \mid g_k^{\text{start}} \in (i, j)\}|,$$

where $\text{Tr} : g_1 \rightarrow g_2 \rightarrow \dots \rightarrow g_{|\text{Tr}|}$ is a trajectory in R , and $g_k^{\text{start}}, g_k^{\text{end}}$ are the geospatial coordinate; $g_k^{\text{start}} \in (i, j)$, $g_k^{\text{end}} \in (i, j)$ mean the trajectory start or end in the grid (i, j) , note that the trajectory can start and end in the same region, $|\cdot|$ denotes the cardinality of a set.

At time interval t , inflows and outflows in all $I \times J$ regions can be denoted by a tensor $\mathbf{X}_t \in R^{2 \times I \times J}$ where $(\mathbf{X}_t)_{0,i,j} = x_t^{\text{in},i,j}$, $(\mathbf{X}_t)_{1,i,j} = x_t^{\text{out},i,j}$. The outflow matrix is shown in Figure 2(a).

Problem 1. Predict \mathbf{X}_n given historical observations $\{\mathbf{X}_t \mid t = 0, \dots, n-1\}$ and external factors such as weather conditions, wind speed, temperature, and day-of-week.

3 Methodology

Input (Zhang, Zheng, and Qi 2017). We sample historical flow videos from recent time to near history and distant history according to three corresponding temporal views: closeness, period, and trend. We select hours, daily, and

weekly as the key timesteps to construct the three views. For each of temporal views, we fetch a list of key timesteps' flow matrices and concatenated them, to construct the input as:

$$\begin{aligned}\mathbf{X}_{\text{closeness}} &= [\mathbf{X}_{t-1}, \mathbf{X}_{t-2}, \dots, \mathbf{X}_{t-l_r}] \in \mathbb{R}^{N \times C \times l_r} \\ \mathbf{X}_{\text{period}} &= [\mathbf{X}_{t-p_d}, \mathbf{X}_{t-2p_d}, \dots, \mathbf{X}_{t-l_d * p_d}] \in \mathbb{R}^{N \times C \times l_d} \\ \mathbf{X}_{\text{trend}} &= [\mathbf{X}_{t-p_w}, \mathbf{X}_{t-2p_w}, \dots, \mathbf{X}_{t-l_w * p_w}] \in \mathbb{R}^{N \times C \times l_w} \\ \{\mathbf{X}_t | t = 0, \dots, n-1\} &= [\mathbf{X}_{\text{closeness}} \mathbf{X}_{\text{period}}, \mathbf{X}_{\text{trend}}],\end{aligned}$$

where l_r, l_d, l_w are input lengths of hours, daily, and weekly, p_d, p_w are daily and weekly periods. We choose l_r, l_d, l_w as 4, 4, 4, in our study.

Decomposition into patches. Similar to Dosovitskiy et al. (2020), we first decompose each frame into N_1 big patches, each of size $2 \times P_1 \times P_1'$ and 2 means outflow and inflow. Then we decompose each big patch into N_2 small patches, each of size $2 \times P_2 \times P_2'$. We obtain N patches, where $N = N_1 \times N_2 = HW/P_2P_2'$. We then flatten these patches of the entire flow videos into vectors $\mathbf{x}_{(p,t)} \in \mathbb{R}^{2 \times P_2 \times P_2'}$, where $p = 1, \dots, N$ denotes spatial localization and $t = 1, \dots, F$ denotes indexes of frames in the flow videos. $F = F_1 \times F_2$ includes F_1 fragments (i.e., closeness, period, trend), and each fragment include F_2 frames, i.e., $F_1 = 3, F_2 = 4$ in our study.

Linear embedding. By means of a learnable matrix $E \in \mathbb{R}^{D \times 2P_2P_2'}$, we linearly map each patch $x_{(p,t)}$ into an embedding vector $\mathbf{z}_{(p,t)}^{(0)} \in \mathbb{R}^D$:

$$\mathbf{z}_{(p,t)}^{(0)} = E\mathbf{x}_{(p,t)} + \mathbf{e}_{(p,t)}^{pos}, \quad (1)$$

where $\mathbf{e}_{(p,t)}^{pos} \in \mathbb{R}^D$ denotes a learnable positional embedding added to encode the spatiotemporal position of each patch. The final sequence of embedding vectors $\mathbf{z}_{(p,t)}^{(0)}$ for $p = 1, \dots, N$ and $t = 1, \dots, F$ represents the input flow videos after preprocessing.

Query-Key-Value. Similar to the BERT Transformer (Devlin et al. 2018), ProSTformer also uses Encoder framework consisting of L encoding blocks. At each block l , a query/key/value vector is computed for each patch from the $\mathbf{z}_{(p,t)}^{(l-1)}$ encoded by the preceding block:

$$\begin{aligned}\mathbf{q}_{(p,t)}^{(l,a)} &= W_Q^{(l,a)} \text{LN} \left(\mathbf{z}_{(p,t)}^{(l-1)} \right) \in \mathbb{R}^{D_h} \\ \mathbf{k}_{(p,t)}^{(l,a)} &= W_K^{(l,a)} \text{LN} \left(\mathbf{z}_{(p,t)}^{(l-1)} \right) \in \mathbb{R}^{D_h} \\ \mathbf{v}_{(p,t)}^{(l,a)} &= W_V^{(l,a)} \text{LN} \left(\mathbf{z}_{(p,t)}^{(l-1)} \right) \in \mathbb{R}^{D_h},\end{aligned} \quad (2)$$

where LN denotes LayerNorm (Ba, Kiros, and Hinton 2016), $a = 1, \dots, A$ is an index over multiple self-attention heads, and A denotes the total number of self-attention heads. The latent dimensionality for each self-attention head is set to $D_h = D/A$.

3.1 Progressive Space-Time self-attention.

We first factorize the dependencies and then propose ProSTformer to focus on spatial dependence from local to

global regions, on temporal dependence from inside to outside fragment (i.e., closeness, period, and trend), and finally on external dependence such as weather, temperature, and day-of-week. In ProSTformer, each block highlights the unique dependence by aggregating the patches with spatiotemporal positions to significantly decrease the self-attention computation. We give a sketch of the self-attention schemes in Figure 3, and provide architecture details in Figure 4.

Local spatial self-attention block. We split each frame into N_1 spatial groups, each of which includes N_2 small patches. Then, we implement self-attention for each small patch in the group, filtering the patches in other groups. In practice, the group dimension N_1 and temporal dimension F are merged into the batch dimension for simplifying the operation. At the end of this block, we rearrange the output back to (B, NF, D) :

$$\text{rearrange}(B, NF, D \rightarrow BN_1F, N_2, D). \quad (3)$$

For each small patch $x_{(p,t)} \in \mathbb{R}^{2 \times P_2 \times P_2'}$ in each frame t' , we only allow each key to attend its adjacent patches' queries:

$$\alpha_{(p,t')}^{(l,a)} = \text{SoftMax} \left(\frac{\mathbf{q}_{(p,t')}^{(l,a)\top} \cdot \mathbf{k}_{(p',t')}^{(l,a)}}{\sqrt{D_h}} \right), \quad (4)$$

where $p = 1, \dots, N$ and $p' = 1, \dots, N_2$, note that p' is dynamically relative to p .

Global spatial self-attention block. After implementing the local spatial self-attention for each small patch, we then implement global spatial self-attention for each big patch in the same frame. In practice, the temporal dimension F is merged into the batch dimension for simplifying the operation. At the end of this block, we rearrange the output back to (B, NF, D) :

$$\text{rearrange}(B, NF, D \rightarrow BF, N_1, N_2D). \quad (5)$$

For each big patch $x_{(p,t)} \in \mathbb{R}^{2 \times P_1 \times P_1'}$ in each frame t' , we allow each key to attend the global patches' queries in Eq. 4, where $p = 1, \dots, N_1$ and $p' = 1, \dots, N_1$.

Inside temporal self-attention block. We split the small patches in the same spatial position into F_1 temporal groups, each of which includes F_2 patches. Then, we implement self-attention for each small patch inside the group, filtering the patches outside the group. In practice, the group dimension F_1 and the spatial dimension N are merged into the batch dimension for simplifying the operation. At the end of this block, we rearrange the output back to (B, NF, D) :

$$\text{rearrange}(B, NF, D \rightarrow BNF_1, F_2, D). \quad (6)$$

For each small patch $x_{(p,t)} \in \mathbb{R}^{2 \times P_2 \times P_2'}$ in the same spatial position p' , we only allow each key to attend the inside patches' queries in the group:

$$\alpha_{(p',t)}^{(l,a)} = \text{SoftMax} \left(\frac{\mathbf{q}_{(p',t)}^{(l,a)\top} \cdot \mathbf{k}_{(p',t')}^{(l,a)}}{\sqrt{D_h}} \right), \quad (7)$$

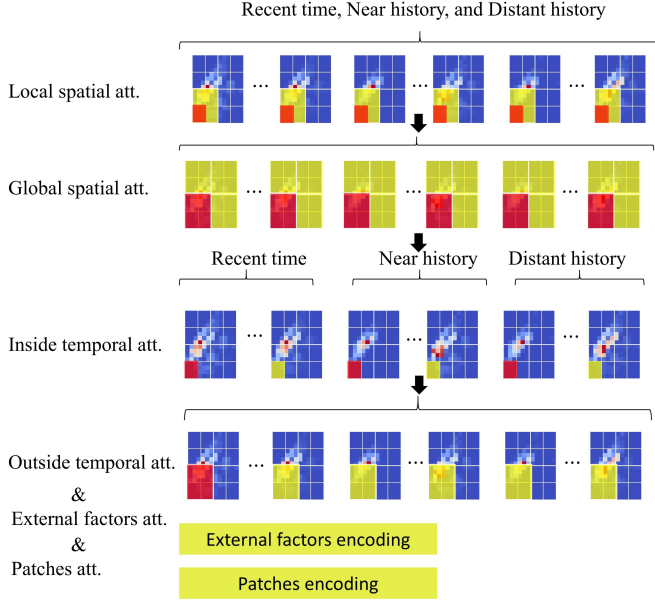


Figure 3: Visualization of the progressive space-time self-attention blocks. Each video is split to a sequence of small patches with a size of 3×4 pixels. We show in red the query patch and show in yellow its spatiotemporal self-attention patches under each block. Patches without color are not used for the self-attention computation of the red patch. Note that self-attention is computed for every single patch in the video clip, i.e., every patch serves as a query. The self-attention pattern extends in the same fashion to all frames of the clip. The external factors and patches self-attention are computed with all patches in the outside temporal self-attention block.

where $t = 1, \dots, F$ and $t' = 1, \dots, F_2$, note that t' is dynamically relative to t .

Outside temporal self-attention block. After implementing the inside temporal self-attention, we then implement the outside temporal self-attention for each big patch in the same spatial position. In practice, the spatial dimension N_1 is merged into the batch dimension for simplifying the operation, at the end of this block, we rearrange the output back to (B, NF, D) :

$$\text{rearrange}(B, NF, D \rightarrow BN_1, F, N_2D). \quad (8)$$

For each big patch $x_{(p,t)} \in \mathbb{R}^{2 \times P_1 \times P'_1}$ in same spatial position p' , we allow each key to attend the patches' queries of all frames in Eq. 7, where $t = 1, \dots, F$ and $t' = 1, \dots, F$.

Encoding. We encode the values of patches in every block. The encoding $\mathbf{z}_{(p,t)}^{(l)}$ at block l are obtained by weighting the sum of value vectors using self-attention coefficients from each self-attention head:

$$\mathbf{s}_{(p,t)}^{(l,a)} = \sum_{p'=1}^N \sum_{t'=1}^F \alpha_{(p,t),(p',t')}^{(l,a)} \mathbf{v}_{(p',t')}^{(l,a)}. \quad (9)$$

Note that we implement spatial self-attention only along the spatial dimension, and the temporal self-attention only

along the temporal dimension. p, p', N, t, t', F have different definitions in each block. Then, we concatenate these vectors from all heads and linearly map it back to patch dimension, using residual connections after LayerNorm:

$$\mathbf{z}'_{(p,t)}^{(l)} = W[\mathbf{s}_{(p,t)}^{(l,a)}, \dots, \mathbf{s}_{(p,t)}^{(l,A)}]^\top \quad (10)$$

$$\mathbf{z}_{(p,t)}^{(l)} = \text{LN}(\mathbf{z}'_{(p,t)}^{(l)}) + \mathbf{z}_{(p,t)}^{(l-1)}. \quad (11)$$

The encoding process is conducted in each self-attention block of ProSTformer. For simplicity, we do not replicate it in each block. In the final outside temporal self-attention block, the output is passed to an MLP layer.

External factors embedding. We linearly map the external factors such as weather, day-of-week, wind speed and temperature into an embedding token [ext] $\mathbf{z}_{ext}^{(l)} \in \mathbb{R}^{N_2D}$, then compute self-attention and encoding with all patches in the outside temporal self-attention block. The output is passed to an MLP layer.

Patches embedding. We extend the concept of token [cls], using N_1 randomly initialized patches token [pat] $\mathbf{z}_{pat}^{(N_1,l)} \in \mathbb{R}^{N_2D}$ to compute self-attention and encoding with all patches in the outside temporal self-attention block. The final prediction $\mathbf{Pre} \in \mathbb{R}^{2 \times H \times W}$ is obtained by combining the [pat] tokens:

$$\mathbf{Pre} = \text{combine}[\mathbf{z}_{pat}^{(n,l)}, \dots, \mathbf{z}_{pat}^{(N_1,l)}]. \quad (12)$$

3.2 ProSTformer Model

We reduce the self-attention computation by replacing with the progressive space-time self-attention in Eq. (3) to (8). For each patch, excluding the [ext] and [pat] self-attention, compared to (NF) times self-attention needed by Vanilla Transformer, ProSTformer only need $(N_2 + N_1 + F_2 + F)$ times self-attention. The encoding $\mathbf{z}_{(p,t)}^{(l)}$ resulting from local spatial self-attention block is then fed to global spatial self-attention block, temporal self-attention block, and outside temporal self-attention block instead of being passed to the MLP. Finally, the encoding of the outside temporal self-attention is passed to the MLP. In each block, new key/query/value vectors are obtained from Eq. (2) and matrices $\{W_{Q_{\text{local}}}^{(l,a)}, W_{K_{\text{local}}}^{(l,a)}, W_{V_{\text{local}}}^{(l,a)}\}$, $\{W_{Q_{\text{global}}}^{(l,a)}, W_{K_{\text{global}}}^{(l,a)}, W_{V_{\text{global}}}^{(l,a)}\}$, $\{W_{Q_{\text{inside}}}^{(l,a)}, W_{K_{\text{inside}}}^{(l,a)}, W_{V_{\text{inside}}}^{(l,a)}\}$, and $\{W_{Q_{\text{outside}}}^{(l,a)}, W_{K_{\text{outside}}}^{(l,a)}, W_{V_{\text{outside}}}^{(l,a)}\}$. To explore the time and space priority for traffic flow forecasting, we also experiment with a progressive “time-space” self-attention model ProTSformer that reverses the time and space priority of ProSTformer.

4 Experiment

4.1 Datasets

We use two datasets, including the trajectory data of yellow taxi and sharing bike in New York City (NYC).

NYCTaxi: The trajectory data is yellow taxi GPS data for New York City (NYC) from 1st Jan. 2013 to 31st Dec. 2015 about 416 million trajectories. We partition

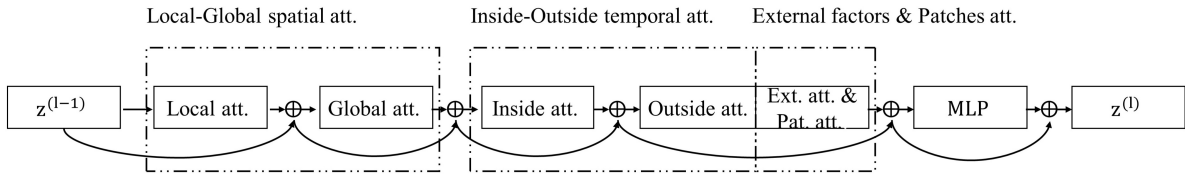


Figure 4: Illustration of the progressive self-attention blocks. We use residual connections to aggregate information from different self-attention layers within each block. A 1-hidden-layer MLP is applied after the outside temporal block. The final model is constructed by repeatedly stacking these blocks on top of each other.

Table 1: The prediction results. ProST[†] is pre-trained on 30 min datasets and then fine tuned on 60 min and 90 min datasets. Other methods have no pre-training.

	Win.	Metrix	HA	ConvLSTM	ST-Res	Trans	Informer	TimeS	ProST	ProST [†]
NYC Taxi	90 min	RMSE	119.32	26.43	15.56	20.97	15.98	20.38	16.71	12.79
		MAE	32.83	7.58	4.91	6.85	5.40	6.82	5.55	4.56
	60 min	RMSE	80.58	34.20	11.32	14.98	11.72	15.09	11.71	10.54
		MAE	22.26	8.49	4.07	5.57	4.45	5.63	4.39	4.01
	30 min	RMSE	40.92	22.14	10.52	13.50	10.30	13.19	10.21	
		MAE	11.45	6.33	3.64	5.10	3.98	4.95	3.82	
NYC Bike	90 min	RMSE	25.62	1.99	2.10	2.09	2.02	2.06	1.99	1.91
		MAE	8.47	0.78	0.85	0.84	0.93	0.86	0.78	0.79
	60 min	RMSE	17.43	4.59	4.06	4.48	4.13	4.44	3.97	3.78
		MAE	5.76	1.66	1.61	1.83	1.72	1.80	1.63	1.61
	30 min	RMSE	8.90	2.30	2.47	2.45	2.34	2.43	2.30	
		MAE	3.00	1.01	1.09	1.10	1.06	1.09	1.04	
Count			0	3	2	0	0	0	3	9

NYC into 12×16 regions. To explore the dataset scale granularity in this problem, we create separate datasets as $\{\text{NYCTaxi}_{30\text{min}}, \text{NYCTaxi}_{60\text{min}}, \text{NYCTaxi}_{90\text{min}}\}$ for 30 minutes, 60 minutes, and 90 minutes time windows.

NYCBike: The trajectory data is sharing bike GPS data for New York City (NYC) from 1st Jan. 2018 to 31th Dec. 2020, about 56 million trajectories. We partition NYC into 12×16 regions, and create separate datasets as $\{\text{NYCBike}_{30\text{min}}, \text{NYCBike}_{60\text{min}}, \text{NYCBike}_{90\text{min}}\}$.

For all datasets, we choose data from the last four weeks as the test set, all data before that as the training set. We remove unavailable bike stations in NYCBike, and the city regions’ partition is same in NYCTaxi and NYCBike.

4.2 Experimental Details

Baselines: We select six forecasting methods as the comparison. For Transformer, TimeSformer, and Informer, we implement the same external factors and patches self-attention with ProSTformer. We split per frame into 16 patches for 12 frames, totally obtain 192 patches as input. All methods have the same input, except that ConvLSTM and HA exclude the external factors.

- **HA :** Historical average, uses the average of previous values in the training dataset as the prediction.
- **ConvLSTM (Xingjian et al. 2015) :** ConvLSTM adds a convolutional structure to LSTM to learn spatiotemporal features.
- **ST-ResNet (Zhang, Zheng, and Qi 2017) :** ST-ResNet

employs convolution-based residual networks to extract spatiotemporal dependence.

- **Transformer (Dosovitskiy et al. 2020) :** Transformer directly learns the spatiotemporal features from a sequence of video patches’ embedding.
- **Informer (Zhou et al. 2021)** Informer designs a ProbSparse self-attention mechanism distilling highlights dominating self-attention by halving cascading layer input.
- **TimeSformer (Bertasius, Wang, and Torresani 2021):** TimeSformer proposes a “divided self-attention”, where the temporal and spatial self-attention are separately applied within each block.

Hyper-parameter tuning: ProSTformer contains 6-layer stack. Similar to the setting in (Dosovitskiy et al. 2020), our method is optimized with Adam optimizer for 1000 epochs, and its learning rate linearly warmup from 0 to $1e-4$ for 200 epochs and then linearly decreases to 0. The batch size is 32 per GPU. The details of baseline methods can be found in Appendix A. **Normalization:** The input of each dataset is Min-Max normalized to the range $[-1, 1]$. **Metrics:** We train all methods with MSE loss, and use two evaluation metrics: $\text{RMSE} = \sqrt{\frac{1}{n} \sum_{i=1}^n (y - \hat{y})^2}$ and $\text{MAE} = \frac{1}{n} \sum_{i=1}^n |y - \hat{y}|$. **Platform:** All the methods were trained/tested on double Nvidia V100 16GB GPUs.

Table 2: The performances of data augmentation tasks on 30 min NYCTaxi dataset. ProST is the benchmark without pre-training.

Tasks	ProST	Rotation	Time-point
RMSE	10.21	10.60	10.19
MAE	3.82	3.99	3.82

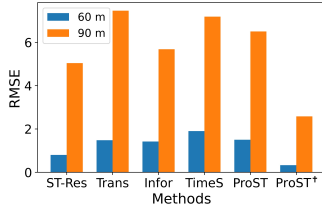


Figure 5: The error increase on NYCTaxi datasets.

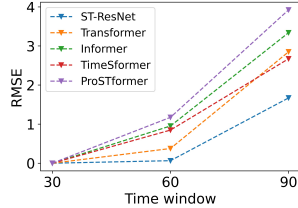


Figure 6: The error decrease with pre-training on NYC-Taxi datasets.

4.3 Results and Analysis

Table 1 summarizes the evaluation results of all methods on two datasets. We gradually prolong the time window on NYCTaxi and NYCBike, a longer time window means a smaller dataset scale, a 30 min dataset contains 52,560 items, a 60 min dataset contains 26,280 items, and a 90 min dataset contains 17,520 items. And we define 30 min datasets as big scale, 60 min datasets as medium scale, and 90 min datasets as small scale.

Forecasting on different time windows and dataset scales. From Table 1, we can observe that: (1) The proposed model ProSTformer[†] that is pre-trained on 30 min datasets, significantly improves the prediction performance (winning-counts in the last column), and its error rises more slowly than other methods with the growing of dataset scale, as shown in Figure 5. (2) Without pre-training, ProSTformer performs better than the relevant TimeSformer, Informer, and Transformer on big scale datasets. (3) Compared with ST-ResNet and ConvLSTM, ProSTformer performs better or the same on big scale datasets by RMSE. On medium and small scale datasets, pre-trained model ProSTformer[†] performs better than them by RMSE. Specifically, compared with ST-ResNet by RMSE. On NYCTaxi, ProSTformer[†] achieves a decrease 3.1% on the big scale dataset, 7.5% on the medium scale dataset, 21.7% on the small scale dataset. On NYCBike, ProSTformer[†] achieves a decrease of 7.0% on the big scale dataset, 7.0% on the medium scale dataset, 9.2% on the small scale dataset.

The importance of pre-training. Without pre-training, the errors of ProSTformer, TimeSformer, Informer, and Transformer increase more rapidly than ST-ResNet on medium and small scale NYCTaxi datasets, as shown in Figure 5. But with pre-training, ProSTformer achieves a significant enhancement, as shown in Figure 6, and the error increase of ProSTformer[†] is the slowest on the medium and small scale NYCTaxi datasets as shown in Figure 5.

The performances of data augmentation tasks. We di-

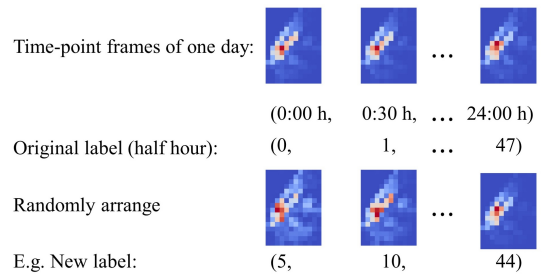


Figure 7: The random arrangement of time-point frames.

rectly pre-train ProSTformer on 30 min datasets, and fine tune it on the 60 min and 90 min datasets, leading to the best performance model ProSTformer[†]. From the perspective of data augmentation, the pre-training on 30 min datasets can be regarded as a closely relevant augmentation task for traffic flow forecasting task on 60 min and 90min datasets. We also conduct additional two data augmentation tasks to pre-train ProSTformer, which are image rotation class task (Gidaris, Singh, and Komodakis 2018) and image time-point class task, as shown in Figure 7, based on 30 min NYCTaxi dataset. From Table 2, we observe that the rotation class task increases the error, and the time-point class task slightly decreases the error. The two tasks do not improve the performances possibly because the two tasks are low relevant to traffic flow forecasting task for extracting the spatiotemporal dependence.

4.4 Fine tune the baseline methods

On account of pre-training significantly improve the performance of ProSTformer, we also implement same pre-training with all the baseline methods.

The effects of pre-training. We observe that: (1) From Table 3, on a total of six datasets, our method obtains top 1 on four datasets and top 2 on the other two datasets by RMSE. On the whole, our method performs best (winning-counts in the last column), and the enhancement of ProSTformer[†] is the most significant with pre-training on NYCTaxi, as shown in Figure 6. (2) Compare Table 1 with Table 3, pre-training almost improves all methods’ performances. With pre-training and shorter input length, Informer, Transformer-s, and TimeSformer-s instead surpass ST-ResNet by RMSE. It shows the convolution-free Transformer-like model’s potential value in traffic flow forecasting.

The priority of space and time. We explore the time and space priority in ProSTformer[†] on different datasets. From Table 3, the space priority model ProSTformer[†] generally performs better (winning-counts in the last column) than the time priority model ProTSformer[†], but ProTSformer[†] performs better on 60 min NYCBike dataset by RMSE.

The performances of different sequence length. We also conduct additional experiments with 48 sequence length for Transformer and TimeSformer rather than 196, which is denoted as “Trans-s” and “TimeS-s” in Table 3. It is shown that the shorter input sequence significantly improves the performances of Transformer and TimeSformer. The results

Table 3: The prediction results with pre-training. All methods are pre-trained on 30 min datasets, and then fine tuned on 60 min and the 90 min datasets. The “-s” indicates the input length is 48 rather than 196 for other models. ProTS[†] reverses the spatial and temporal blocks of ProST[†].

	Win.	Metrix	ConvLSTM	ST-Res	Trans	Trans-s	Informer	TimeS	TimeS-s	ProTS [†]	ProST [†]
MAE	6.92	4.79	6.11	4.70	4.69	4.69	6.09	4.76	4.84	4.56	
60 min	RMSE	33.41	11.26	14.61	10.91	10.77	14.24	10.78	10.92	10.54	
	MAE	7.96	4.14	5.44	4.14	4.35	5.40	4.13	4.22	4.01	
30 min	RMSE	22.14	10.52	13.50	10.43	10.30	13.19	10.29	10.64	10.21	
	MAE	6.33	3.64	5.10	3.89	3.98	4.95	3.89	4.01	3.82	
NYC Bike	90 min	RMSE	1.92	1.98	2.04	1.89	1.91	2.03	1.89	1.93	1.91
		MAE	0.76	0.80	0.83	0.78	0.83	0.82	0.77	0.78	0.79
	60 min	RMSE	4.51	4.12	4.33	3.74	3.76	4.30	3.72	3.71	3.78
		MAE	1.62	1.65	1.76	1.58	1.65	1.75	1.56	1.58	1.61
	30 min	RMSE	2.30	2.47	2.45	2.30	2.34	2.43	2.30	2.32	2.30
		MAE	1.01	1.09	1.10	1.03	1.06	1.09	1.03	1.04	1.04
Count			3	1	2	1	3	6			

Table 4: Ablation study of each block. ProST is the benchmark of no ablation.

Block ablation	ProST	No the local block	No the global block	No the Inside block	No the Outside block
RMSE	10.21	10.24	10.25	10.24	10.36
MAE	3.82	3.88	3.80	3.86	3.84

Table 5: Ablation study of decomposition ways.

Decomposition ways	Way 1	Way 2	Way 3
RMSE	10.21	10.35	10.30
MAE	3.82	3.86	3.82

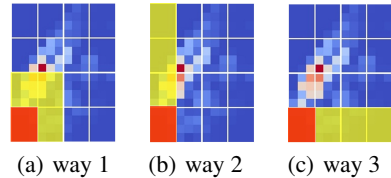


Figure 8: The decomposition ways. We show in red the query patch and show in yellow its local spatial self-attention patches.

verify the assumption that there are redundant dot-product pairs of the low relevant patches. ProSTformer[†] performs well on the long input sequence, we attribute it to that the progressive self-attention mechanism significantly decrease the redundant computation. Informer also performs well on the long input sequence, because its distilling mechanism effectively filters the redundant computation.

4.5 Ablation Study

We also conducted additional experiments on 30 min NYCTaxi dataset with ablation consideration for ProSTformer.

The performance of each block. We explore the influence of each block in ProSTformer by eliminating the local, global, inside, and outside self-attention block, respectively. The other experimental setups are aligned with the settings of ProSTformer. From Table 4, ProSTformer achieves the best performance than the ablation version models by RMSE. We conclude that the progressive space-time self-attention mechanism is worth adopting.

The performances of decomposition ways. In Table 1, 2, 3, and 4, we use way 1 in Figure 8(a) to decompose the flow videos and implement the self-attention in ProSTformer. The decomposition way indicates the adjacent patches of a patch to implement the local-global spatial self-attention. The spatial self-attention blocks will influence the

following temporal blocks due to the subsequent encoding pass. We conduct additional experiments with decomposition way 2 and way 3, as shown in Figure 8(b) and 8(c), to explore the decomposition ways influence. From Table 5, way 1 intuitively and practically performs better than way 2 and way 3 by RMSE.

5 Conclusion

In this paper, we propose ProSTformer for traffic flow forecasting. We first factorize the dependencies and then design a corresponding progressive space-time self-attention mechanism to extract the dependencies. The mechanism incorporates the structure information of the flow videos to significantly decrease the self-attention computation. We show that pre-training is of great importance on medium scale and small scale datasets for Transformer-like models. The experiments on real-world datasets demonstrate that ProSTformer enhances the prediction capacity significantly.

References

- Ba, J. L.; Kiros, J. R.; and Hinton, G. E. 2016. Layer normalization. *arXiv preprint arXiv:1607.06450*.
- Beltagy, I.; Peters, M. E.; and Cohan, A. 2020. Longformer: The long-document transformer. *arXiv preprint arXiv:2004.05150*.
- Bertasius, G.; Wang, H.; and Torresani, L. 2021. Is Space-Time Attention All You Need for Video Understanding? *arXiv preprint arXiv:2102.05095*.
- Chen, Y.; Zou, X.; Li, K.; Li, K.; Yang, X.; and Chen, C. 2021. Multiple local 3D CNNs for region-based prediction in smart cities. *Information Sciences*, 542: 476–491.
- Child, R.; Gray, S.; Radford, A.; and Sutskever, I. 2019. Generating long sequences with sparse transformers. *arXiv preprint arXiv:1904.10509*.
- Devlin, J.; Chang, M.-W.; Lee, K.; and Toutanova, K. 2018. Bert: Pre-training of deep bidirectional transformers for language understanding. *arXiv preprint arXiv:1810.04805*.
- Dosovitskiy, A.; Beyer, L.; Kolesnikov, A.; Weissenborn, D.; Zhai, X.; Unterthiner, T.; Dehghani, M.; Minderer, M.; Heigold, G.; Gelly, S.; et al. 2020. An image is worth 16x16 words: Transformers for image recognition at scale. *arXiv preprint arXiv:2010.11929*.
- Du, B.; Peng, H.; Wang, S.; Bhuiyan, M. Z. A.; Wang, L.; Gong, Q.; Liu, L.; and Li, J. 2019. Deep irregular convolutional residual LSTM for urban traffic passenger flows prediction. *IEEE Transactions on Intelligent Transportation Systems*, 21(3): 972–985.
- Duan, W.; Jiang, L.; Wang, N.; and Rao, H. 2019. Pre-Trained Bidirectional Temporal Representation for Crowd Flows Prediction in Regular Region. *IEEE Access*, 7: 143855–143865.
- Gidaris, S.; Singh, P.; and Komodakis, N. 2018. Unsupervised representation learning by predicting image rotations. *arXiv preprint arXiv:1803.07728*.
- Ke, J.; Zheng, H.; Yang, H.; and Chen, X. M. 2017. Short-term forecasting of passenger demand under on-demand ride services: A spatio-temporal deep learning approach. *Transportation Research Part C: Emerging Technologies*, 85(June): 591–608.
- Kitaev, N.; Kaiser, L.; and Levskaya, A. 2020. Reformer: The efficient transformer. *arXiv preprint arXiv:2001.04451*.
- Li, S.; Jin, X.; Xuan, Y.; Zhou, X.; Chen, W.; Wang, Y.-X.; and Yan, X. 2019. Enhancing the locality and breaking the memory bottleneck of transformer on time series forecasting. *Advances in Neural Information Processing Systems*, 32: 5243–5253.
- Lin, H.; Jia, W.; Sun, Y.; and You, Y. 2019. Spatial-temporal self-attention network for flow prediction. *arXiv preprint arXiv:1912.07663*.
- Xingjian, S.; Chen, Z.; Wang, H.; Yeung, D.-Y.; Wong, W.-K.; and Woo, W.-c. 2015. Convolutional LSTM network: A machine learning approach for precipitation nowcasting. In *Advances in neural information processing systems*, 802–810.
- Yao, H.; Tang, X.; Wei, H.; Zheng, G.; Yu, Y.; and Li, Z. 2018. Modeling spatial-temporal dynamics for traffic prediction. *arXiv preprint arXiv:1803.01254*.
- Zhang, J.; Zheng, Y.; and Qi, D. 2017. Deep spatio-temporal residual networks for citywide crowd flows prediction. In *Thirty-first AAAI conference on artificial intelligence*.
- Zhang, J.; Zheng, Y.; Qi, D.; Li, R.; and Yi, X. 2016. DNN-based prediction model for spatio-temporal data. In *Proceedings of the 24th ACM SIGSPATIAL international conference on advances in geographic information systems*, 1–4.
- Zhang, K.; Liu, Z.; and Zheng, L. 2019. Short-term prediction of passenger demand in multi-zone level: Temporal convolutional neural network with multi-task learning. *IEEE transactions on intelligent transportation systems*, 21(4): 1480–1490.
- Zheng, Y.; Capra, L.; Wolfson, O.; and Yang, H. 2014. Urban computing: concepts, methodologies, and applications. *ACM Transactions on Intelligent Systems and Technology (TIST)*, 5(3): 1–55.
- Zhou, H.; Zhang, S.; Peng, J.; Zhang, S.; Li, J.; Xiong, H.; and Zhang, W. 2021. Informer: Beyond efficient transformer for long sequence time-series forecasting. In *Proceedings of AAAI*.